Research Square

Preprints are preliminary reports that have not undergone peer review.
They should not be considered conclusive, used to inform clinical practice,
or referenced by the media as validated information.

Widespread submarine volcanic eruptions and tectonics revealed in the northwest Pacific Ocean

Lianxing Wen

lianxing.wen@stonybrook.edu

Stony Brook University https://orcid.org/0000-0002-5344-6212

Juan Zhu

University of Science and Technology of China https://orcid.org/0000-0001-9524-614X

Article

Keywords:

Posted Date: October 1st, 2025

DOI: https://doi.org/10.21203/rs.3.rs-7502124/v1

License: This work is licensed under a Creative Commons Attribution 4.0 International License.
Read Full License

Additional Declarations: There is **NO** Competing Interest.

Widespread submarine volcanic eruptions and tectonics revealed in the northwest Pacific Ocean

Juan Zhu[1], Lianxing Wen[2*]

[1]Laboratory of Seismology and Physics of Earth's Interior, School of Earth and Space Sciences, University of Science and Technology of China; Hefei, 230026, China.

[2]Department of Geosciences, State University of New York at Stony Brook; NY 11794, USA.

[*]Correspondence to: Lianxing.Wen@stonybrook.edu

Abstract

Notwithstanding submarine volcanic eruptions carrying crucial information on the tectonics of Earth and volcanic hazards in the ocean, they are inadequately studied and poorly characterized. Here, we report detection of three types of submarine volcano totaling 6208 eruptions from 2010-2022 in the northwest Pacific Ocean based on hydroacoustic data, with the subduction-related volcanoes in the Izu-Bonin and Mariana Arcs and West Mata, the rift-related volcanoes in the Mariana Back-Arc spreading center, Kyushu-Palau Ridge, and both subduction- and rift-related volcanoes at the junction of the Izu-Bonin and Mariana Arcs and the Mariana Back-Arc spreading center. The detected widespread submarine volcano eruptions reveal vastly under-cataloged undersea volcanic hazards and delineate a back-arc formation system in the western Mariana Trench evolving from initial arc forming and arc splitting to a mature back-arc system.

Main Text

A complete knowledge of submarine volcanic eruptions is critical for assessing volcanic hazards in the oceans and improving our understanding of the magmatic and tectonic evolutions of the Earth. Submarine volcanic eruptions could trigger large tsunamis and landslides, and release ashes and volatiles that have huge impacts on the chemistry of atmosphere, marine ecosystem, and health of the population[1]. They could also carry significant information about source process of submarine volcano eruptions[1-5], dynamic process of mid-ocean spreading[6], and tectonics of back-arc formation system which is studied mostly based on the morphology and geographic distribution of arcs and ridges in the back-arc basins[7-12].

Explosive submarine volcano eruptions have been studied based on various types of the observations associated with the eruptions. Researchers have used satellite photography, flyover photos, remotely operated underwater vehicles, autonomous underwater vehicles and chemical sampling to capture explosive submarine volcanic eruption productions, through detections of water discoloration, bathymetry change, lava flow, pumice raft and ash-steam plume[2,5,12-15]. Some researchers have also used the passive observations from ocean bottom seismometers (OBSs) and hydrophones to detect and locate explosive submarine volcanic eruptions[2-4,6,16-21]. However, the catalog of submarine volcanic eruptions remains vastly incomplete and those detected eruptions are poorly characterized. The detections through physical and chemistry changes associated with the eruptions were only performed in certain locations and in some periods of time, and lacked the information on exact location, magnitude and style of the eruptions[1]. The studies based on the OBS data were limited in localized detections around the deployment and by the sparse deployments of OBS stations[1]. Hydrophone data analyses, which rely on the low-frequency sound waves that propagate tens of thousands of kilometers with low energy attenuation in the Sound Fixing and Ranging

(SOFAR) Channel of the ocean (i.e., T-phases), can detect explosive submarine volcanic signals at long distances and provide more complete information about the occurrence, source characteristics, and spatial and temporal distributions of submarine volcano[17-19,21], but those studies remained limited. The lack of a complete knowledge of submarine volcanic activities hinders our understanding of the tectonics and volcanic hazards beneath the ocean.

In this study, we systematically study submarine volcanic activity beneath the northwest Pacific Ocean from 2010-2022, outline a framework of tectonic evolution in the region afforded by the detected volcanic activity, and discuss the implications to the volcanic hazards in the ocean.

Widespread explosive submarine volcanic eruptions beneath the northwest Pacific Ocean

We study occurrence, spatial-temporal distribution and energy release of explosive submarine volcanic eruptions beneath the northwest Pacific Ocean, based on the pressure data recorded in two subarrays of a hydrophone array (H11S and H11N) in the Wake Island operated by the Comprehensive Nuclear-Test-Ban Treaty Organization (CTBTO) (Supplementary Note 1). Volcano event detection follows three steps: 1) potential volcanic T-phase signals are first detected in the data based on three seismic discriminants for a submarine volcano: an impulsive waveform, an inversed dispersion of frequency and an irregular slow-decaying spectrum (Methods; Extended Data Figs. 1-2 and Supplementary Figs. 2-3); 2) the signals due to air-gun shots and other disturbed sources are eliminated from those potential signals (Supplementary Note 2); and 3) many detected explosive submarine volcanic eruptions are independently confirmed by the observational eruption evidence of discolored surface ocean water and ash-steam plumes (Supplementary Note 3). Volcano location is determined by fitting the backazimuths determined based on the H11S and H11N hydrophone data and arrival time

differences observed between two subarrays (Methods; Extended Data Fig. 3). Volcano source level (SL) of an explosive submarine volcanic eruption is defined as the relative strength with respect to a reference source located 1 m away from the hydrophone array[22,23] and is determined based on the amplitudes of the observed T-phase signals and event distance. The acoustic energy E of an eruption is calculated by integrating the acoustic intensity of its signal over source region and signal duration time (Methods). The number of explosive submarine volcanic eruptions (N) in general exhibits an exponential increase with increasing SL toward a certain transitional source level (SL_c) followed an exponential decrease with increasing SL. We characterize the *N*-*SL* relationship with three parameters of SL_c, K_1 and K_2:

$$\begin{cases} log_{10}^{N} = a_1 + K_1 \cdot SL \ \ (SL < SL_c) \\ log_{10}^{N} = a_2 - K_2 \cdot SL \ (SL \geq SL_c) \end{cases} \quad (1)$$

where K_1 and K_2 are the parameters characterizing the event number increase and decrease below and above SL_c respectively, and a_1 and a_2 are constants.

A total of 6208 explosive submarine volcanic eruptions are detected from 2010-2022 in the northwest Pacific Ocean. Those eruptions occur in two different tectonic environments: 1) regions of an oceanic plate subduction under another oceanic plate including Kaitoku, Kita-Ioto, Ioto and Fukutoku-Okanoba in the Izu-Bonin Arc, Daikoku, Ahyi, Agrigan, South Sarigon and NW Rota-1 in the Mariana Arc, and one region in West Mata, and 2) rift regions inside an oceanic plate including three spreading segments at 18.2°N, 17.0°N and 15.5°N in the Mariana Back-Arc spreading center, and one region of the Kyushu-Palau Ridge at 16.3°N of the Philippine Sea (Fig. 1). Volcanoes in these two tectonic environments are termed as subduction-related and rift-related volcanoes respectively.

The rift-related volcanoes erupt frequently with a smaller magnitude (termed as category R). Note that those volcanoes erupt across thirteen years of the study (panels R1-R4, Fig. 2), with the maximum energy release of 49 t TNT (Extended Data Fig. 4) and a narrow distribution of source level ($K2$ reaching up to 0.2) (panels R1-R4, Fig. 3). Those explosive events also exhibit similar distributions of temporal behavior and source level in all three regions of the Mariana Back-Arc spreading center (Figs. 2, 3), indicating a similar magmatic process occurring in the spreading centers. The magma process in the rift environment likely involves decompression melting as the hot mantle material ascends to shallow depths during the rifting[24-27]. As a result, the magma in the rift environment is less influenced by the oceanic crust and possesses a low viscosity, making eruptions being frequent and having a small magnitude. Our detection of the frequent active submarine volcanic eruptions verifies the Mariana Back-Arc spreading center is currently undergoing magmatic extension and delineates detailed source level, source characteristics, and spatial and temporal distributions of the eruptions in the region.

The subduction-related volcanoes can be divided into two categories in accordance with the eruption frequency of the sequence, with one category that erupts sporadically with a relatively large source level (termed as category A) and the other category that exhibit the characteristics of the rift-related volcanoes but with a relatively larger source level (termed as category AR).

Category A volcanoes occur in Kaitoku and Kita-Ioto in the Izu-Bonin Arc, Ahyi, South Sarigon, NW Rota-1, Daikoku and Agrigan in the Mariana Arc and West Mata (Fig. 1). Note that Kaitoku, Kita-Ioto, Ahyi, South Sarigon and NW Rota-1 erupt only in a small number of days, and Daikoku, Agrigan and NW Rota-1 erupt sparsely across thirteen years (Fig. 2). Category A volcanos exhibit varying levels of energy release (K_2 less than 0.12), with those in Kaitoku, Kita-Ioto, Ahyi and South Sarigon having energy releases higher than 300 t TNT, and

those in Daikoku and Agrigan, NW-Rota 1 having relatively low energy releases less than 50 t TNT (Extended Data Fig. 4). The temporal distribution and source characteristics of those category A volcanoes can be attributed to the magmatic process of the subduction-related volcanoes, which likely involves release of volatiles from the subducted plate at large depths with the induced magma ascending through the overlaying oceanic crust. The influence of the silicates in the crust would increase the viscosity of the magma and trap the magma in the crust for a long period of time, making eruptions being sporadic and having a high source level[28,29].

Category AR volcanoes consist of Fukutoku-Okonoba and Ioto volcanoes at the junction of the Izu-Bonin Arc, the Mariana Arc and the Mariana Back-Arc spreading center. The Fukutoku-Okonoba and Ioto volcano sequences exhibit a similar temporal characteristic with those of the rift-related category R volcanos in that they all erupt frequently in the time period from 2010 to 2022 (c.f. AR1-AR2 to R1-R4, Fig. 2). They also exhibit a similar characteristics of source level as those in the subduction-related category A volcanos in that they have high energy releases reaching up to 800 t TNT (Extended Data Fig. 4) and a wide distribution of source level ($K2$ less than 0.12) (c.f. AR1-AR2 to A1-A8, Fig. 3). Based on the observed temporal and source characteristics, we infer that the category AR volcanoes involve two magmatic processes, with one related to typical subduction-related volcanoes and the other related to typical rift-related volcanoes.

Back-arc formation system in western Mariana Trench

Our systematic detection of explosive submarine volcanic eruptions delineates a tectonic framework of the Mariana Back-Arc region from the volcano activities in the region. The subduction-related volcanoes (categories A and AR volcanoes) along the Izu-Bonin Arc and Mariana Arc confirm a volcanically active frontal arc related to the subducted slabs, the rift-

148 related volcanoes (category R volcanoes) along the Marina Back-Arc spreading center confirm
149 active rifting of the back-arc basin, and no explosive volcano activities observed along the
150 West Mariana Ridge confirm the ridge being a remnant arc (Fig. 4a). In particular, the
151 detections of category AR volcanos at Ioto and Fukutoku-Okonoba at the junction of the frontal
152 Izu-Bonin Arc and Mariana Arc, the rifting Marina Back-Arc spreading center and the remnant
153 West Mariana Ridge provide a direct confirmation of the splitting events before the formation
154 of the three types of arcs and reveal that the northward extension of the splitting process of
155 back-arc formation to Ioto (Fig. 4a). We propose the following tectonic evolution model in the
156 region (Figs. 4a, 4b). The back-arc formation starts from subduction-related category A
157 volcanos forming an arc, to category AR volcanoes splitting the arc in back-arc initiation at
158 Ioto and Fukutoku-Okonoba at the junction of Mariana Arc and West Mariana Ridge, and to a
159 mature back-arc system after rifting consisting of the active frontal Mariana Arc formed by
160 subduction-related category A volcanos, the active Mariana Back-arc rift formed by category
161 R volcanos, and a passive remnant west Mariana Ridge that was split from the frontal Mariana
162 Arc and rifted away by the active Mariana Back-arc spreading center.
163

164 **Implications to volcanic hazard beneath the oceans**

165 Periodic multidisciplinary cruises carried out in El Hierro, NW Rota-1, West Mata, Axial
166 Seamount and East Pacific Rise have reported extreme eruption-induced physical and chemical
167 perturbations of sea water including thermal changes, water acidification, deoxygenation and
168 metal-enrichment, and related significant alterations to the activity and composition of local
169 plankton communities[30-32]. Our results however indicate that explosive submarine volcano
170 eruptions occur more frequently than previously thought and the related volcanic hazards are
171 vastly underestimated. Our study also suggests that hydroacoustic monitoring provides a new
172 way to more completely assess submarine volcano hazard in the oceans, by providing detailed

magnitudes, durations, and spatial and temporal distributions of submarine volcanic eruptions beneath the global oceans.

Methods

Detection of explosive submarine volcanic eruption

The detection of explosive submarine volcanic eruptions is based on identification of T-phase signals associated with the eruptions in the hydroacoustic data recorded from 1 January, 2010 to 13 December, 2022 by the H11 hydrophone array located near the Wake Island of the Northwest Pacific Ocean (Supplementary Note 1). The identification consists of three steps: we first detect T-phase signals that stand above the noise level in the data; we identify and retain T-phase signals that exhibit characteristics of an explosive submarine volcanic eruption; and we remove T-phase signals related to air-gun shots and other disturbed sources.

We detect T-phase signals using the Progressive Multi-Channel Correlation (PMCC) method[33]. The PMCC method detects a potential signal based on waveform similarity and traveltime differences between pairs of stations in an array. The detection criteria are adopted for signals generated by a source in a long distance away from the hydrophone array and assume a two-dimensional plane wave propagation of the signals. If signals recorded by all the three stations are from the same source, summation (termed as closure value) of the residuals of traveltime differences between all three station pairs should be close to zero and the cross-correlation coefficients between the observed waveforms in all the three pairs of stations should be close to 1[34]. The observed traveltime differences between the station pairs are obtained from the cross-correlations of their recorded waveforms. In practice, we detect T-phase signals in each sliding 20-s time window with an overlap of 5 s in the pressure data recorded by the H11S

hydrophone subarray. We set three criteria for T-phase signal detection: (1) the inverted wave propagation velocity is within 1.4-1.6 km/s, a bound of water sound velocity of T-phase in the SOFAR channel of ocean[17,19]; (2) the absolute closure value is less than 12 data sampling intervals of 48 ms adopted from the value used in Metz and Grevemeyer[19] and Metz, et al.[20] for IMS hydrophone arrays in the Pacific Ocean; and (3) the average value of the cross-correlation coefficients between waveform pairs of all three stations is larger than 0.3. All the detected T-phase signals are further checked by a detection algorithm based on the ratio of a short-time-average (STA) of waveform energy over a long-time-average (LTA) of waveform energy (STA/LTA)[35], with the durations of STA and LTA set to be 1 s and 3 s, and the STA/LTA triggered and detriggered threshold levels set to be 2.0 and 0.4 respectively. In the last step, we only retain detections that have the left signal-to-noise ratio (SNR) and right SNR larger that 2.0 (left SNR is defined as the ratio of squared amplitude summation in the triggered time window to that of a time window of same duration proceeding the earliest triggered time, while right SNR is defined as the ratio of squared amplitude summation in the triggered time window to that of a time window of same duration starting at the latest detriggered time).

T-signals of an explosive submarine volcanic eruption differ from those of earthquakes in waveform and spectrum[1,15,17,19,21] (Extended Data Fig. 1). T-signals of an explosive submarine volcanic eruption have a short energy duration of less than 5.0 s and a broadband source frequency spectrum ranging 6-60 Hz (Extended Data Fig. 1b), while those of earthquakes exhibit a long energy duration over 20 s and a low-frequency source spectrum with energy concentrated in the frequencies less than 20 Hz (Extended Data Figs. 1c-1d). We identify potential T-phase signals of explosive submarine volcanic eruptions based on three hydroacoustic features in the pressure recordings: 1) an impulsive pressure waveform[36-38], 2) an inversed frequency dispersion of the recorded signals with the high-frequency energy

leading the low-frequency energy in time[38], and 3) an irregular and slowly decaying spectral amplitude of the signals[37]. Accordingly, we define three seismic discriminants (Extended Data Fig. 2): 1) a discriminant characterizing the impulsive feature of the recorded waveform: $D = log_{10}e_{max} - 5.0log_{10}\tau_{1/3} + 4.53$ where e_{max} is the maximum amplitude of the pressure envelope and $\tau_{1/3}$ is the duration the pressure envelope is sustained at or above 1/3 of e_{max}; 2) a discriminant characterizing an inversed dispersion of frequency of the recorded signal: δt the median arrival time difference between the peak of the energy envelope in a low frequency range of 6-10 Hz and the peak of the energy envelope in a high frequency range of 15-25 Hz; and 3) a set of discriminants characterizing the decay (α) and irregularity (r^2) of the signal spectrum in which α is the parameter of a function $A(f) = Cf^{-\alpha}$ (C is a constant) that best fits the observed spectrum $A_o(f)$ and r^2 is the maximum cross-correlation coefficient between $ln\ A(f)$and $ln\ f$ in a frequency range of 6-30 Hz, i.e., $\frac{\int_6^{30} lnA_o(f)\cdot ln(f+\xi)d\xi}{\sqrt{\int_6^{30} ln\ A_o(\xi)d\xi}\cdot\sqrt{\int_6^{30} ln\xi d\xi}}$. We regard the signals to be associated with a potential explosive submarine volcanic eruption when these three discriminants satisfy the following conditions: 1) positive D values in three H11S hydrophone recordings, 2) positive δt values in three H11S hydrophone recordings, and 3) $\alpha < 1.5$ and $r^2 < 0.8$ in a minimum of two H11S hydrophone observations. We show an example of signal identification of a potential explosive submarine volcanic eruption at hydrophone station H11S1 (event 1, Extended Data Fig. 1b), with a positive D value of 3.92 (Extended Data Fig. 2a), a positive δt value of 0.72 s (Extended Data Fig. 2b), and a set of ($\alpha < 1.06$; $r^2 < 0.63$) (Extended Data Fig. 2c) (see Supplementary Figs. 2, 3 for the consistent three discriminants based on H11S2 and H11S3 hydrophone data).

Location determination of explosive submarine volcanic eruption

We determine the horizontal location of an explosive submarine volcanic eruption based on best fitting the backazimuths of the event inferred separately from the H11S and H11N hydrophone data based on the PMCC technique[33] and observed differential arrival times of the signals between the two hydrophone subarrays. We grid-search the best-fitting source location along the inferred backazimuth direction based on the H11S hydrophone data starting from the center of the hydrophone array. At each test source location, we define a root mean square (RMS) residual ε of backazimuth and arrival time difference as:

$$\varepsilon=\sqrt{\frac{(Baz_{pre}^{N}-Baz_{infer}^{N})^2+(Baz_{pre}^{S}-Baz_{infer}^{S})^2+W*(\Delta t_{pre}^{S-N}-\Delta t_{obs}^{S-N})^2}{3}} \quad (2)$$

where N and S represent the northern and southern hydrophone subarrays, Baz_{pre}^{N} and Baz_{pre}^{S} are the predicted backazimuth from the test source location to the hydrophone subarrays, Baz_{infer}^{N} and Baz_{infer}^{S} are the inferred backzimuths based on the data in the two hydrophone subarrays, Δt_{pre}^{S-N} is the difference of predicted arrival times between the H11S and H11N hydrophone subarrays from the test source location, Δt_{obs}^{S-N} is the observed arrival time difference of the signals between the H11S and H11N hydrophone subarrays, and W is a weighting factor of the arrival time residual relative to the backazimuth residuals.

We admit a test location as an acceptable event location when $\varepsilon \leq 1.0$. Location uncertainties are determined to be the region of 95% confidence level of the minimal residual based on the chi-square distribution of ε. We show source location determination using event 1 as an example (Extended Data Fig. 3). We infer a backazimuth of 288.18° of the event based on the H11S hydrophone data. We perform source location searches along the inferred backazimuth direction and obtain the best-fitting horizontal location of $(141.37°E,\ 24.27°N)$ with an ε of 0.097 (Extended Data Fig. 3). The uncertainties of the event source location are estimated to

be 350 km along the direction of the inferred backazimuth and 20 km in the direction perpendicular to the inferred backazimuth. The best-fitting location is less than 10 km away from a region of observed discolored water on the sea surface and the inferred event origin time is within two minutes of the observed time of discoloring (Supplementary Fig. 7).

Source level, energy release, and uncertainties of source level distribution of explosive submarine volcanic eruptions

Source level (SL) of an explosive submarine volcanic eruption, as defined by the relative strength with respect to a reference source located 1 m away from the hydrophone array[22,23], is estimated as:

$$SL = 20\ log(P/P_0) + \ 20\ log\ (r/r_0) \quad (3)$$

where P is the maximal pressure signals recorded in the hydrophone, P_0 is the reference pressure of 1 μPa, r is the distance between the event and the hydrophone, r_0 is the reference distance of 1 m. The second term of equation (3) accounts for the propagation loss from the event. The unit of SL is $dB\ re\ 1\mu$Pa at 1m.

The acoustic energy E of an eruption is calculated by integrating the acoustic intensity of its signal over source region and signal duration time[19,39,40], i.e.:

$$E = I \times 2\pi\ \times T \quad (J) \quad (4)$$

where T is the duration of the signal, I is the acoustic intensity defined as $I = \frac{SL^2}{Z}$ with Z being the specific acoustic impedance of sea water (the product of a nominal density of 1,030 kg/m^3 and a sound velocity of 1450 m/s of sea water), and 2π is the geometric factor by assuming the energy is released into an acoustic half-space.

The standard errors of K_1 and K_2 value in the *N-SL* relationship in equation (1), i.e., δK_1 and δK_2, are estimated following Shi and Bolt[41] and Tan, et al.[42]:

$$\begin{cases} \delta K_1 = 2.3{K_1}^2\sqrt{\frac{\sum_i^c (SL_i-\overline{SL_l})^2}{c(c-1)}} & (i < c) \\ \delta K_2 = 2.3{K_2}^2\sqrt{\frac{\sum_i^n (SL_i-\overline{SL_h})^2}{(n-c)(n-c-1)}} & (i \geq c) \end{cases} \quad (5)$$

where SL_i is the source level of the ith eruption, n is the total eruption sample size, c is the sample point of SL_c, $\overline{SL_l}$ is the mean SL of explosive events with $SL < SL_c$, and $\overline{SL_h}$ is the mean *SL* of explosive events with $SL \geq SL_c$.

References

1 Tepp, G. & Dziak, R. P. The seismo‐acoustics of submarine volcanic eruptions. *Journal of Geophysical Research: Solid Earth* **126**, e2020JB020912 (2021).

2 Chadwick Jr, W. *et al.* Direct video and hydrophone observations of submarine explosive eruptions at NW Rota‐1 volcano, Mariana arc. *Journal of Geophysical Research: Solid Earth* **113** (2008).

3 Searcy, C. Seismicity associated with the may 2010 eruption of South Sarigan Seamount, northern Mariana Islands. *Seismological Research Letters* **84**, 1055-1061 (2013).

4 Wilcock, W. S. *et al.* Seismic constraints on caldera dynamics from the 2015 Axial Seamount eruption. *Science* **354**, 1395-1399 (2016).

5 Chadwick Jr, W. W. *et al.* Recent eruptions between 2012 and 2018 discovered at west mata submarine volcano (NE Lau Basin, SW Pacific) and characterized by new ship, AUV, and ROV data. *Frontiers in Marine Science*, 495 (2019).

6 Tan, Y. J., Tolstoy, M., Waldhauser, F. & Wilcock, W. S. Dynamics of a seafloor-spreading episode at the East Pacific Rise. *Nature* **540**, 261-265 (2016).

7 Karig, D. E. Ridges and basins of the Tonga‐Kermadec island arc system. *Journal of geophysical research* **75**, 239-254 (1970).

8 Stern, R. J., Fouch, M. J. & Klemperer, S. L. An overview of the Izu-Bonin-Mariana subduction factory. *Geophysical Monograph-American Geophysical Union* **138**, 175-222 (2003).

9 Anderson, M. O. *et al.* Geological interpretation of volcanism and segmentation of the M ariana back‐arc spreading center between 12.7° N and 18.3° N. *Geochemistry, Geophysics, Geosystems* **18**, 2240-2274 (2017).

10 Taylor, B. *Backarc basins: Tectonics and magmatism*. (Springer Science & Business Media, 2013).

11 Fryer, P. Geology of the Mariana trough. *Backarc basins: Tectonics and magmatism*, 237-279 (1995).

12 Chadwick Jr, W. W. *et al.* A recent volcanic eruption discovered on the central Mariana back-arc spreading center. *Frontiers in Earth Science* **6**, 172 (2018).
13 Maeno, F. *et al.* Seawater-magma interactions sustained the high column during the 2021 phreatomagmatic eruption of Fukutoku-Oka-no-Ba. *Communications Earth & Environment* **3**, 260 (2022).
14 Yoshida, K. *et al.* Variety of the drift pumice clasts from the 2021 Fukutoku‐Oka‐no‐Ba eruption, Japan. *Island Arc* **31**, e12441 (2022).
15 Matsumoto, H. *et al.* Interpretation of detections of volcanic activity at Ioto Island obtained from in situ seismometers and remote hydrophones of the International Monitoring System. *Scientific Reports* **9**, 19519 (2019).
16 Dziak, R. P. & Fox, C. G. Evidence of harmonic tremor from a submarine volcano detected across the Pacific Ocean basin. *Journal of Geophysical Research: Solid Earth* **107**, ESE 1-1-ESE 1-11 (2002).
17 Green, D. N. *et al.* Hydroacoustic, infrasonic and seismic monitoring of the submarine eruptive activity and sub-aerial plume generation at South Sarigan, May 2010. *Journal of Volcanology and Geothermal Research* **257**, 31-43 (2013).
18 Metz, D., Watts, A. B., Grevemeyer, I., Rodgers, M. & Paulatto, M. Ultra‐long‐range hydroacoustic observations of submarine volcanic activity at Monowai, Kermadec Arc. *Geophysical Research Letters* **43**, 1529-1536 (2016).
19 Metz, D. & Grevemeyer, I. Hydroacoustic measurements of the 2014 eruption at Ahyi volcano, 20.4 N Mariana Arc. *Geophysical Research Letters* **45**, 11,050-011,058 (2018).
20 Metz, D., Watts, A., Grevemeyer, I. & Rodgers, M. Tracking submarine volcanic activity at Monowai: Constraints from long‐range hydroacoustic measurements. *Journal of Geophysical Research: Solid Earth* **123**, 7877-7895 (2018).
21 Tepp, G. *et al.* Hydroacoustic, seismic, and bathymetric observations of the 2014 submarine eruption at Ahyi seamount, Mariana Arc. *Geochemistry, Geophysics, Geosystems* **20**, 3608-3627 (2019).
22 Page, C. H. & Vigoureux, P. *The international system of units (SI)*. Vol. 330 (US Department of Commerce, National Bureau of Standards, 1974).
23 Miksis-Olds, J. L., Harris, D. V. & Heaney, K. D. Comparison of estimated 20-Hz pulse fin whale source levels from the tropical Pacific and Eastern North Atlantic Oceans to other recorded populations. *The Journal of the Acoustical Society of America* **146**, 2373-2384 (2019).
24 CArEy, S. & SigurdSSoN, H. Exploring submarine arc volcanoes. *Oceanography* **20**, 80-89 (2007).
25 White, R. S. & McKenzie, D. P. Volcanism at rifts. *Scientific American* **261**, 62-71 (1989).
26 Head III, J. W., Wilson, L. & Smith, D. K. Mid‐ocean ridge eruptive vent morphology and substructure: Evidence for dike widths, eruption rates, and evolution of eruptions and axial volcanic ridges. *Journal of Geophysical Research: Solid Earth* **101**, 28265-28280 (1996).
27 Tolstoy, M. Mid‐ocean ridge eruptions as a climate valve. *Geophysical Research Letters* **42**, 1346-1351 (2015).
28 Cañón-Tapia, E. & Walker, G. P. Global aspects of volcanism: the perspectives of "plate tectonics" and "volcanic systems". *Earth-Science Reviews* **66**, 163-182 (2004).
29 Passarelli, L. & Brodsky, E. E. The correlation between run-up and repose times of volcanic eruptions. *Geophysical Journal International* **188**, 1025-1045 (2012).

30 Santana-Casiano, J. M. *et al.* The natural ocean acidification and fertilization event caused by the submarine eruption of El Hierro. *Scientific reports* **3**, 1140 (2013).
31 Carey, R. J., Butterfield, D. A. & Clark, M. R. Submarine Volcanic Eruptions and Their Impacts on Hydrothermal Systems and Biological Communities. *Annual Review of Earth and Planetary Sciences* **53**, 397-423 (2025).
32 Resing, J. A. *et al.* Chemistry of hydrothermal plumes above submarine volcanoes of the Mariana Arc. *Geochemistry, Geophysics, Geosystems* **10** (2009).
33 Cansi, Y. An automatic seismic event processing for detection and location: The PMCC method. *Geophysical research letters* **22**, 1021-1024 (1995).
34 Graeber, F. M. & Piserchia, P. F. Zones of T‐wave excitation in the NE Indian ocean mapped using variations in backazimuth over time obtained from multi‐channel correlation of IMS hydrophone triplet data. *Geophysical Journal International* **158**, 239-256 (2004).
35 Trnkoczy, A. in *New Manual of Seismological Observatory Practice (NMSOP)* 1-20 (Deutsches GeoForschungsZentrum GFZ, 2009).
36 Talandier, J. & Okal, E. A. Seismic detection of underwater volcanism: The example of French Polynesia. *pure and applied geophysics* **125**, 919-950 (1987).
37 Reymond, D., Hyvernaud, O., Talandier, J. & Okal, E. A. T-wave detection of two underwater explosions off Hawaii on 13 April 2000. *Bulletin of the Seismological Society of America* **93**, 804-816 (2003).
38 Talandier, J. & Okal, E. A. A new source discriminant based on frequency dispersion for hydroacoustic phases recorded by T-phase stations. *Geophysical Journal International* **206**, 1784-1794 (2016).
39 Hildebrand, J. A. Anthropogenic and natural sources of ambient noise in the ocean. *Marine Ecology Progress Series* **395**, 5-20 (2009).
40 Bohnenstiehl, D. R., Dziak, R. P., Matsumoto, H. & Conder, J. A. Acoustic response of submarine volcanoes in the Tofua Arc and northern Lau Basin to two great earthquakes. *Geophysical Journal International* **196**, 1657-1675 (2014).
41 Shi, Y. & Bolt, B. A. The standard error of the magnitude-frequency b value. *Bulletin of the Seismological Society of America* **72**, 1677-1687 (1982).
42 Tan, Y. J., Waldhauser, F., Tolstoy, M. & Wilcock, W. S. Axial Seamount: Periodic tidal loading reveals stress dependence of the earthquake size distribution (b value). *Earth and Planetary Science Letters* **512**, 39-45 (2019).
43 Tozer, B. *et al.* Global bathymetry and topography at 15 arc sec: SRTM15+. *Earth and Space Science* **6**, 1847-1864 (2019).
44 Global Volcanism Program. [Database] Volcanoes of the World (v. 5.2.2; 22 Aug 2024). *Distributed by Smithsonian Institution, compiled by Venzke, E.*, doi:https://doi.org/10.5479/si.GVP.VOTW5-2024.5.2 (2024).
45 Resing, C. S. J., Chadwick, W. & Volz, C. H. FK151121-Hydrothermal Hunt on the Mariana Back-arc. (2016).

Declarations

Data availability Hydroacoustic data are available by the CTBTO International Data Centre, Vienna, through the virtual Data Exploitation Centre (vDEC, available at https://www.ctbto.org/specials/vdec/). The catalogs of earthquakes are available by the USGS (available at https://www.usgs.gov/) and ISC (available at https://www.isc.ac.uk/). The topographical data is from the 15 Arc-Second Global Relief Model[43] (SRTM15+, available at https://topex.ucsd.edu/WWW_html/srtm15_plus.html).

Acknowledgments We gratefully acknowledge Yen Joe Tan, William W. Chadwick Jr., Gabrielle Tepp and Xiao Xiao for fruitful discussions. This work is supported by the National Natural Science Foundation of China under grants NSFC42130301 and NSFC42250201.

Author contributions L.W. designed and supervised the project, J.Z. performed technical analyses of explosive submarine volcanic eruptions.

Competing interests The authors declare that there are no competing interests. The views expressed herein are those of the authors and do not necessarily reflect the views of the CTBTO Preparatory Commission.

Correspondence and requests for materials should be addressed to Lianxing Wen.

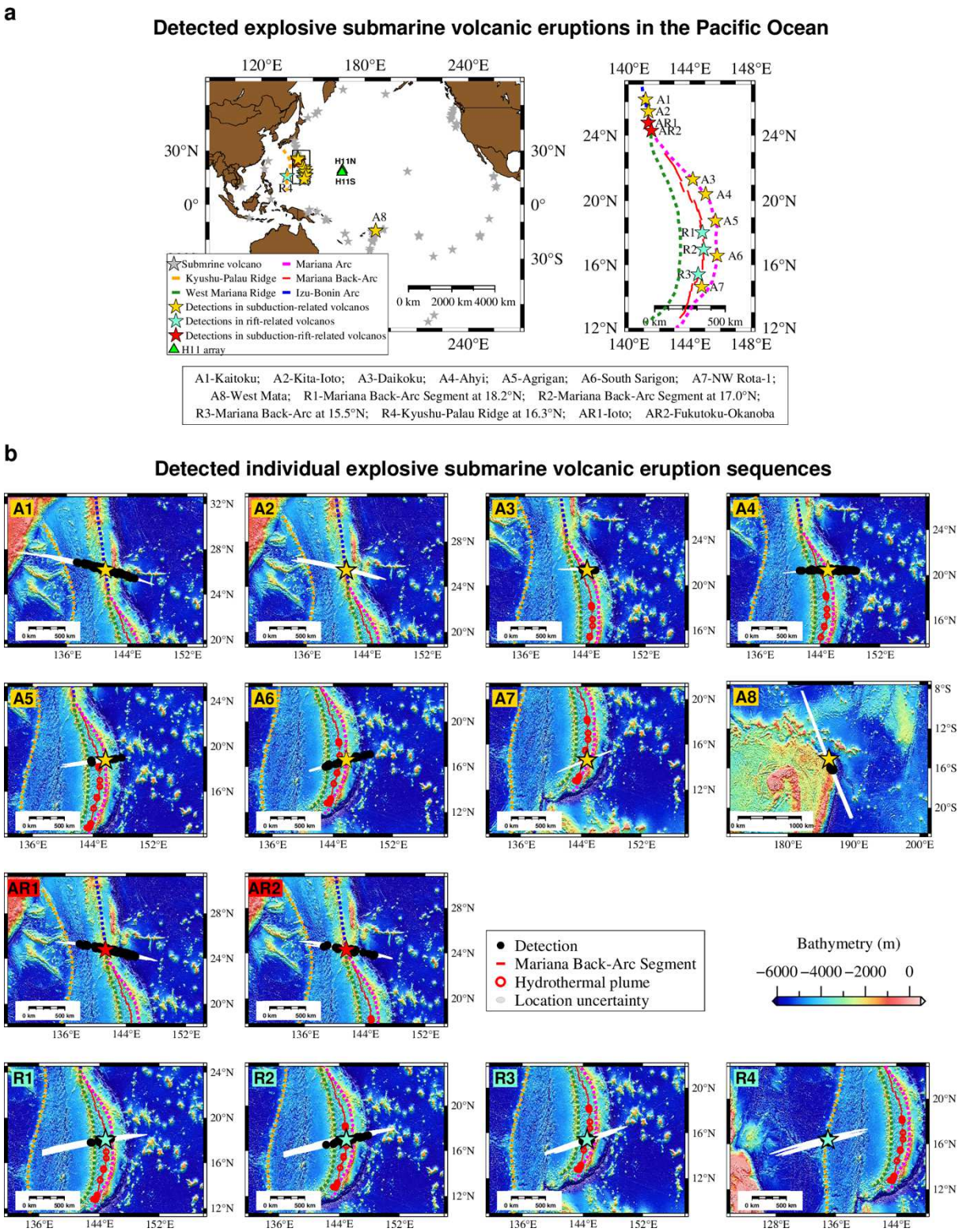

438

439 **Fig. 1 | Detected explosive submarine volcanic eruptions in the northwest Pacific Ocean.**

440 **a**, (Left) Detected explosive submarine volcanic eruptions (color stars), in the Izu-Bonin Arc

441 (red and yellow stars), Mariana Arc (yellow stars), Mariana-Back Arc (lightblue stars),

442 Kyushu-Palau Ridge (lightblue star) and West Mata (yellow star), along with known submarine

volcanos (grey stars)[44]. Black box indicates the enlarged region in the right panel. H11N and H11S hydrophone subarrays are indicated by green triangles. The Kyushu-Palau Ridge is marked as orange dashed curve. (Right) Detected explosive submarine volcanic eruption regions along the Mariana Island (black box in the left panel), with each region labeled by alphabets (A for arc, R for rift, AR for arc and rift) followed by a number. The Izu-Bonin Arc, Mariana Arc, Mariana Back-Arc spreading center, West Mariana Ridge are marked as blue, magenta, red and green dashed curves, respectively. **b**, Detected explosive submarine volcanic eruptions (black dots) in **a**, with sub-panels labeled accordingly with the regions in **a** and volcanos (stars) color-coded with the stars in **a**. White ellipses represent location errors of the events. Red solid circles mark the locations of hydrothermal plumes in the Mariana Back-Arc[45]. Background color marks bathymetry.

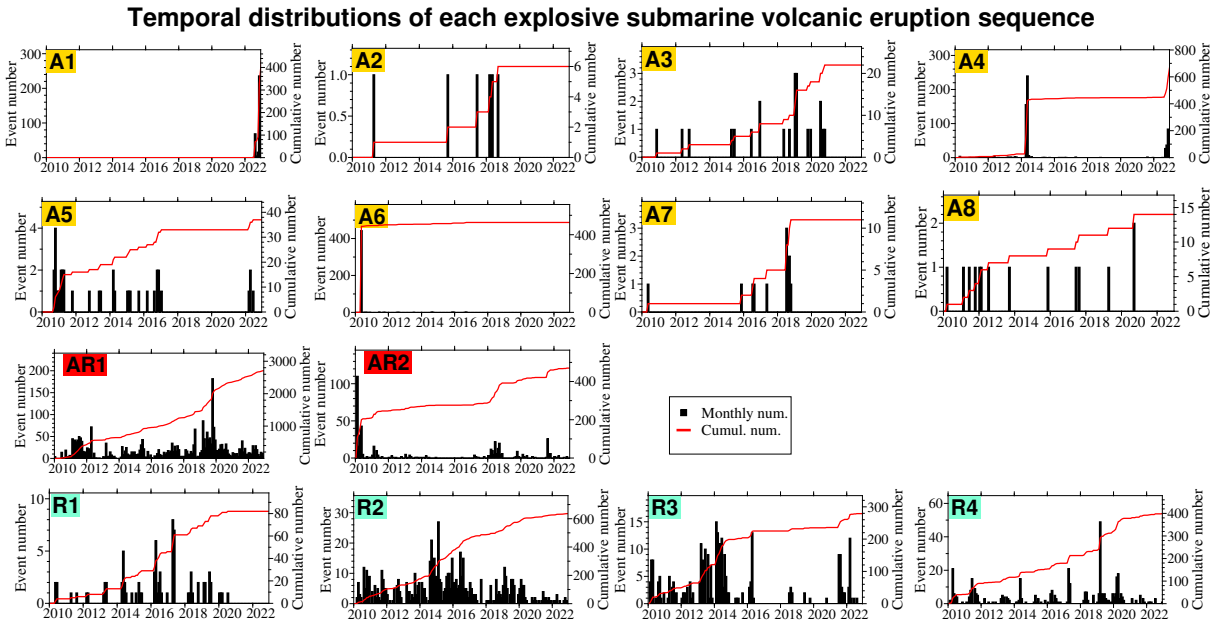

Fig. 2 | Detected explosive submarine volcanic eruptions in regions of the northwest Pacific Ocean from 2010 to 2022. Each sub-panel is for eruptions in a geographical region, labeled accordingly to those in Fig. 1. In each sub-panel, bars show the monthly numbers of the detected eruptions with the scale indicated in the left vertical axis and the red curve shows the cumulative numbers of eruptions with the scale indicated in the right vertical axis.

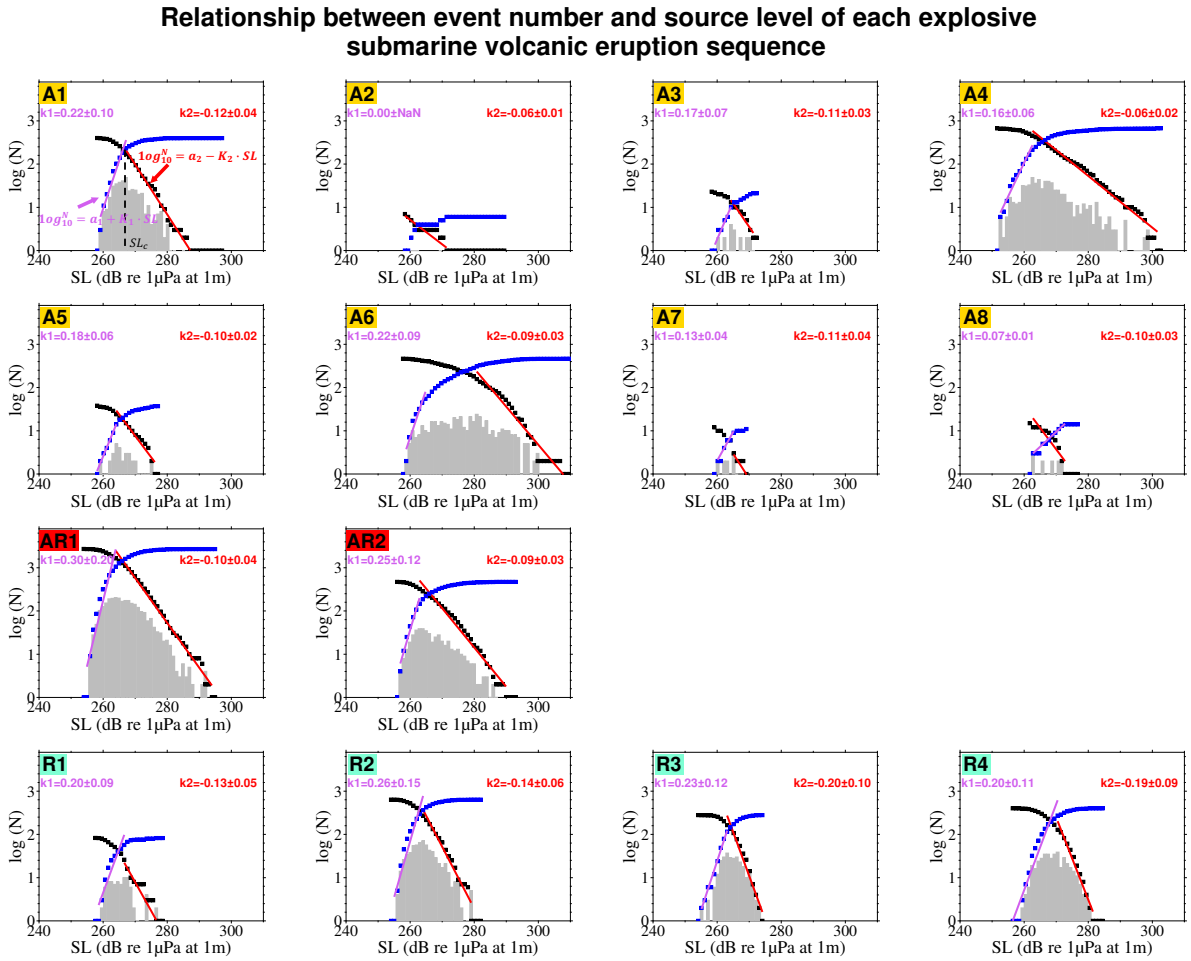

462

463 **Fig. 3 | Relationship between event number and source level in each explosive submarine**
464 **volcanic eruption sequence.** Each sub-panel is for eruptions in a geographical region, labeled
465 accordingly to those in Fig. 1. In each sub-panel, grey bars represent histograms of event
466 number (N) with respect to source level (SL) within a bin of 1 $dB\ re\ 1\mu Pa\ at\ 1m$, black and
467 blue dots show the cumulative numbers of events below and above each source level
468 respectively, and purple and red lines present the best-fitting exponentially increasing and
469 decreasing functions (with the equations labeled as purple and red, and the transitional source
470 level SL_c indicated by black vertical dashed line in sub-panel "A1") to the histograms of event
471 number below and above each source level respectively ($K1\ and\ K2$ of the best-fitting
472 exponential functions are labeled in the top of the panels).

473

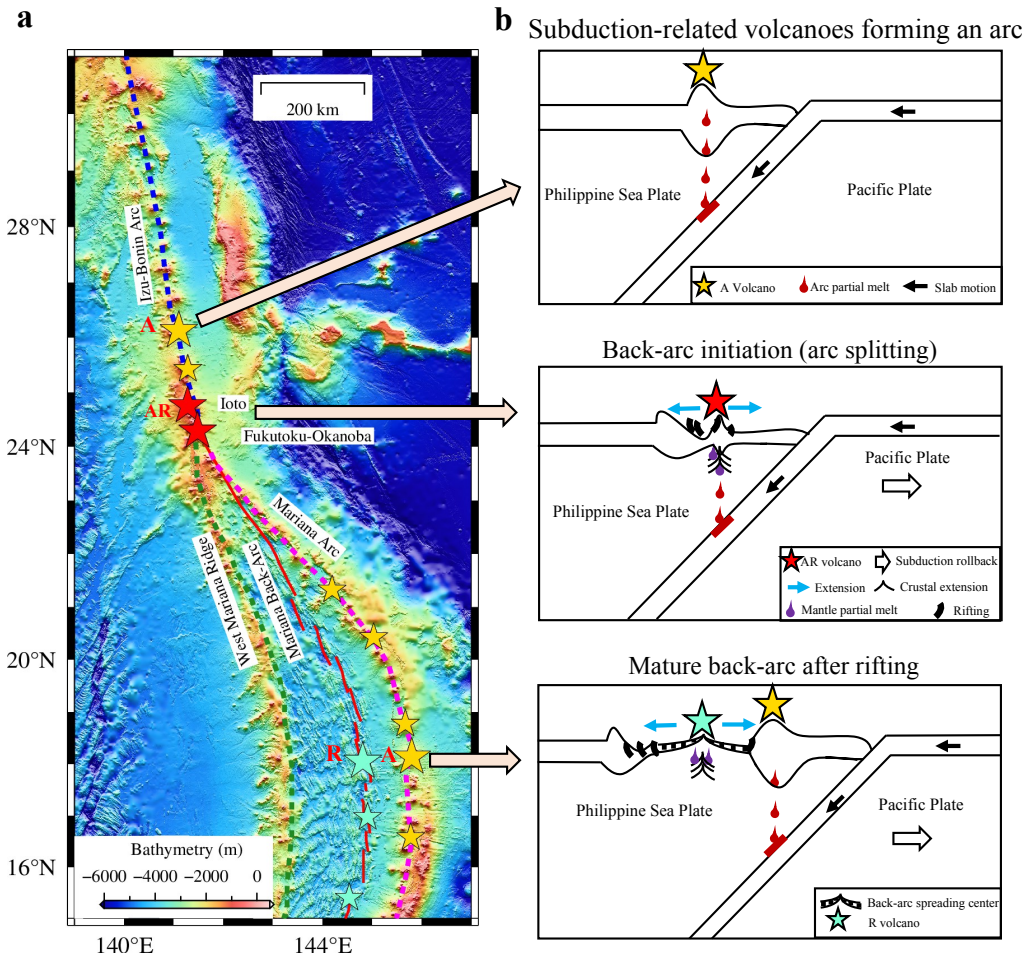

474

475 **Fig. 4 | Cartoon illustrating tectonic evolution of the Mariana Back-Arc formation based**
476 **on detected submarine volcanoes. a**, Detected submarine volcanoes (stars) and three example
477 A, AR, and R volcanos (labeled with large stars) to illustrate a proposed tectonic evolution
478 model of the Mariana Back-Arc formation in **b**. The Izu-Bonin Arc, Mariana Arc, Mariana
479 Back-Arc spreading center, West Mariana Ridge are marked as blue, magenta, red and green
480 dashed curves respectively. Background color marks bathymetry. **b**, A proposed tectonic
481 evolution model of the Mariana Back-arc formation, starting from (top) subduction-related
482 category A volcanos forming an arc, to (middle) arc splitting by category AR volcanoes in
483 back-arc initiation at the junction of Mariana Arc and West Mariana Ridge, and to (bottom) a
484 mature back-arc system after rifting consisting of the active frontal Mariana Arc formed by
485 subduction-related category A volcanos, the active Mariana Back-Arc rift formed by category

R volcanos, and a passive remnant west Mariana Ridge that was split from the frontal Mariana Arc and rifted away by the active Mariana Back-Arc rift.

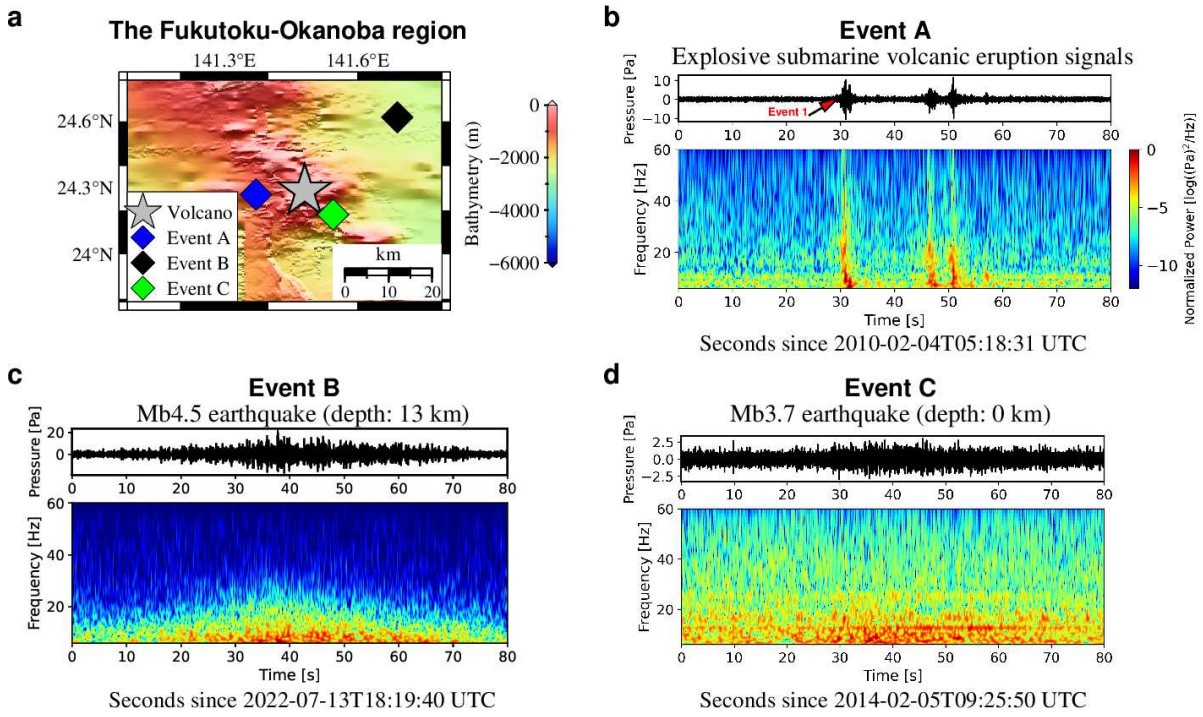

Extended Data Fig. 1 | Waveform and spectrogram of example events of three different types around Fukutoku-Okanoba. a, Locations of three example events, including an explosive submarine volcanic eruption (event A, blue rhombus), a Mb 4.5 earthquake of a reported source depth of 13 km (event B, black rhombus), and a Mb 3.7 earthquake of a reported depth of 0 km (event C, blue rhombus). The Fukutoku-Okanoba seamount is marked with grey star. Background color marks bathymetry. **b-d**, Pressure waveforms recorded at hydrophone station H11S1 (top) and the associated spectrograms (bottom) for (**b**) event A, (**c**) event B and (**d**) event C. Red arrow in **b** indicates event 1 that is used to show the procedures of event identification in Extended Data Fig. 2 and Supplementary Figs. 2-3, and location determination in Extended Data Fig. 3.

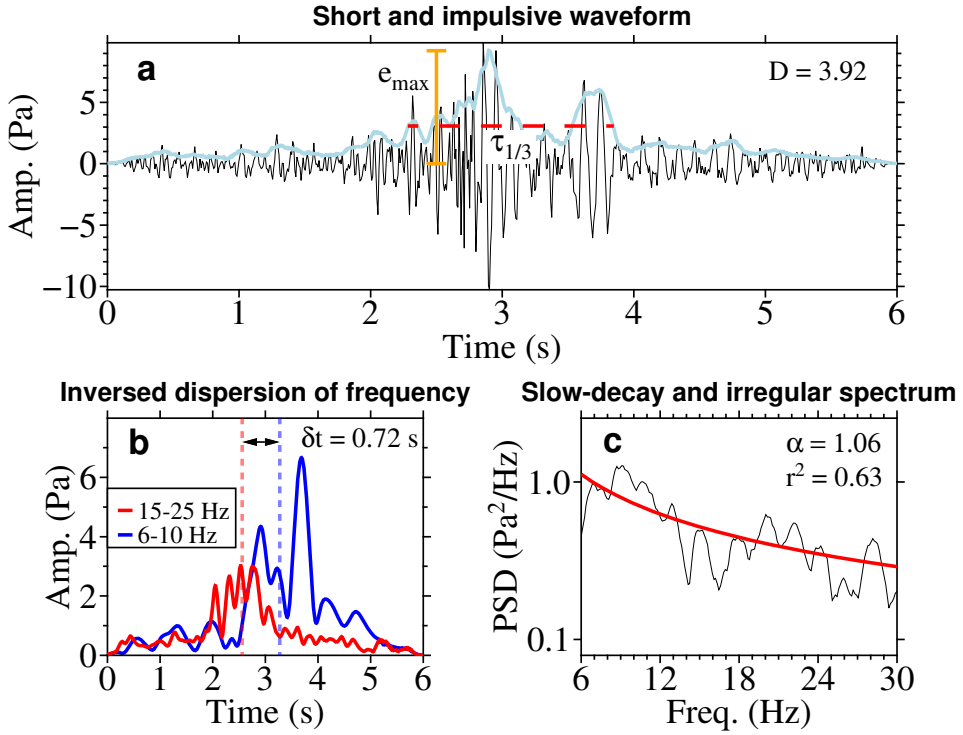

501

502 **Extended Data Fig. 2 | Detection discriminants for an explosive submarine volcanic**
503 **eruption. a**, Discriminant D with the value labeled in the right-top panel, and associated e_{max}
504 indicated by gold vertical bar on the pressure envelope (blue curve) and $\tau_{1/3}$ indicated by the
505 length of red horizontal dashed line of amplitude level of 1/3 of e_{max}. Pressure envelop is
506 obtained from smoothing the waveform (black trace) with a bin of 0.2 s. **b**, δt (length of black
507 horizontal arrow and valued labeled in the right-top panel), with red curve for the pressure
508 envelop in a high-frequency range of 15-25 Hz and blue curve for the pressure envelop in a
509 low-frequency range of 6-10 Hz. Vertical dashed lines are the arrival time picks for the
510 envelopes at or above 1/3 of the e_{max}, color-coded with the envelops in two frequency ranges.
511 **c**, (α, r^2) with values labeled in the right-top of the panel, with red curve representing function
512 $A(f) = Cf^{-\alpha}$ and black curve representing the observed spectrum $A_0(f)$. The record is from
513 hydrophone station H11S1 for an example event occurring at 05:19:01 UTC, on February 4,
514 2010 (event 1, Extended Data Fig. 1).

515

516

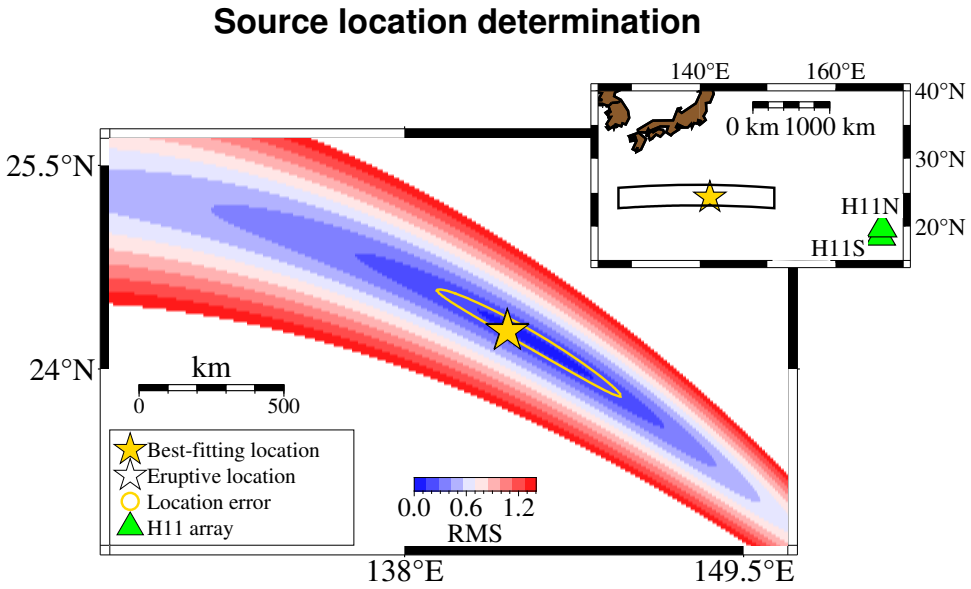

Extended Data Fig. 3 | Location determination of an explosive submarine volcanic eruption. RMS residuals ε (color background W = 0.25 in equation (2)) between calculated and observed backazimuths and arrival time delays at H11N and H11S, as a function of potential event location. Gold star shows the best-fitting event location with the minimum RMS residual ε, gold ellipse indicates the location uncertainties with an error of 350 km along the direction of the inferred backazimuth and 20 km in the direction perpendicular to the inferred backazimuth. White star indicates the location of lotus-pattern discolored water observed at 04:51 UTC on February 4, 2010 by a local flyover (photo in Supplementary Fig. 7). (Right-top inset) The region of the main figure (black rectangle) in a broader region of the Pacific Ocean and northern and southern hydrophone subarrays (green triangles, labeled as H11N and H11S respectively) around the Wake Island. The event occurs at 05:19:01 UTC, on February 4, 2010 (event 1, Extended Data Fig. 1).

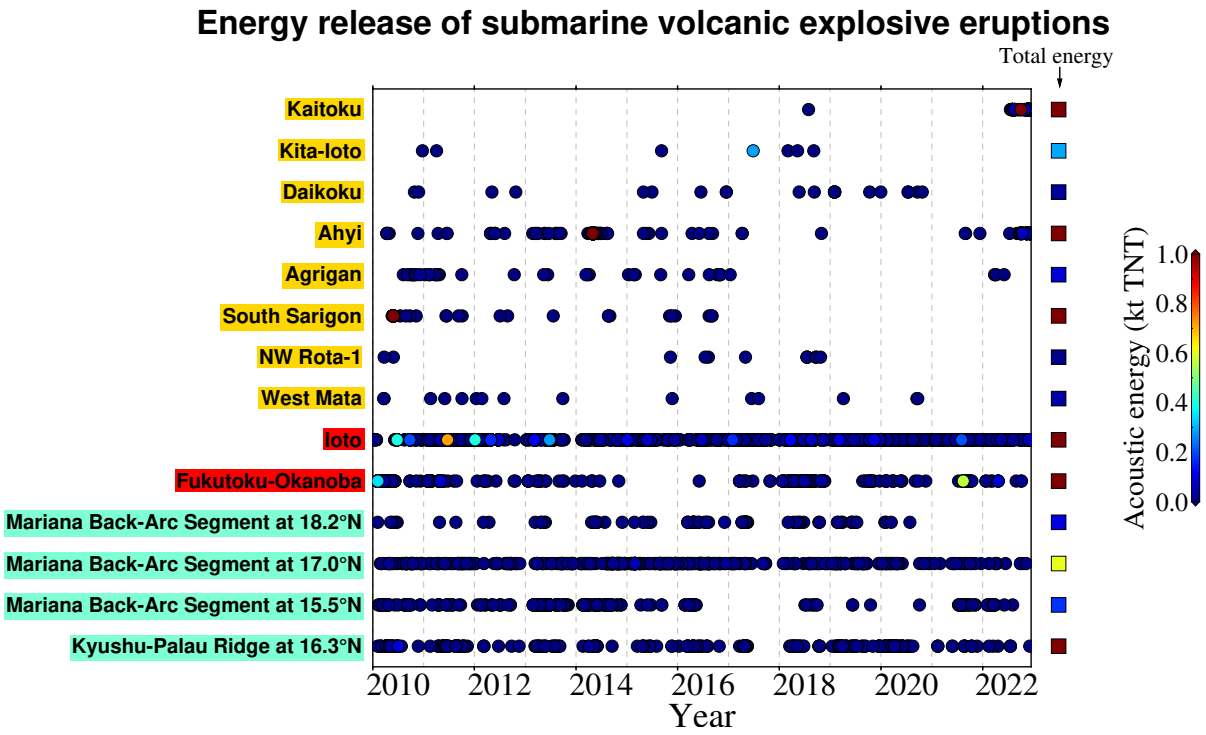

531

532 **Extended Data Fig. 4 | Energy release of explosive submarine volcanic eruptions.** Each
533 dot shows an explosive submarine volcanic eruption and squares on the right are used to
534 represent the total acoustic energy levels of each volcano sequence. Background colors of dots
535 and squares represent energy level. Regions of volcano eruptions are labeled accordingly to
536 those in Fig. 1.

537

Supplementary Files

This is a list of supplementary files associated with this preprint. Click to download.

- SupplementaryInformation.pdf